Tailored cancer therapy by magnetic nanoparticle hyperthermia: A virtual scenario simulation method

Roberto Montes-Robles [a], Hazael Montanaro [c,d], Myles Capstick [c], Javier Ibáñez-Civera [a], Rafael Masot-Peris [a], Eduardo García-Breijo [a], Nicolás Laguarda-Miró [a,*], Ramón Martínez-Máñez [a,b,c]

[a] Interuniversity Research Institute for Molecular Recognition and Technological Development (IDM), Universitat Politècnica de València (UPV), Universitat de València (UV), Valencia, Spain
[b] CIBER in the Subject Area of de Bioengineering, Biomaterials and Nanomedicine (CIBER-BBN), Madrid, Spain
[c] ITIS Foundation for Research on Information Technologies in Society, Zurich, Switzerland
[d] Swiss Federal Institute of Technology (ETHZ), Zurich, Switzerland

ARTICLE INFO

ABSTRACT

Background and objective: Hyperthermia is a cancer treatment aiming to induce cell death by directly warming cancerous tissues above 40 °C. This technique can be applied both individually and together with other cancer therapies. The main challenge for researchers and medics is to heat only tumoral cells avoiding global or localized heating of sane tissues. The objective in this study is to provide a realistic virtual scenario to develop an optimized multi-site injection plan for tailored magnetic nanoparticle-mediated hyperthermia applications.
Methods: A three-dimensional model of a cat's back was tested in three different simulation scenarios, showing the impact of magnetic nanoparticles in each specific environment configuration.
Results: As a result of this study. This simulation method can, minimising the affection to healthy tissue.
Conclusions: This virtual method will help real and personalized therapy planning and tailor the dose and distribution of magnetic nanoparticles for an enhanced hyperthermia cancer treatment.

1. Introduction

Hyperthermia is the fourth recognised cancer therapy technique after surgery, chemotherapy and radiation [1]. This technique is minimally invasive and consists of heating a tumoral tissue up to 40–48 °C [2]. Clinical studies confirm that hyperthermia produces a noteworthy toxicity in tumour cells and induces apoptosis [3,4] as well as a synergetic effect when combined with radio or chemotherapy [5]. In fact, improvement factors in the range 1.5 to 5 have been reported when used together with radiotherapy and up to 10 when combined with chemotherapy [6].

Modern techniques permit the performance of improved local hyperthermia therapies minimizing the effects on the surrounding healthy tissue [7,8]. In this sense, the newest radiofrequency devices (RF) remarkably improve the hyperthermia results [5] by increasing the penetration of the radio waves and focusing on a specific tissue volume being both directly related to the selected wavelengths. As a result, a precise and comparatively large heated volume is obtained [9]. In this technique, reflection, coupling, and absorption are different for each case and depend on the tumour location, requiring a specific planning for each patient and making it difficult to obtain a perfect setup. Whereas, focused ultrasound devices are able to heat very precise volumes; these volumes are much smaller than the tumour, which requires a step-and-repeat approach [10]. This coverage complicates the therapy, particularly if the patient moves during the treatment.

On the contrary, hyperthermia therapy mediated by direct injection of magnetic nanoparticles (MNPs) does not exhibit the afore-mentioned problems [11]. MNPs are excited by low frequency electromagnetic field (LF-EMF) irradiation, releasing the energy as heat [12,13]. In this technique, LF-EMF itself does not significantly contribute to tissue heating, as the loss mechanisms are small for the low intensity and frequency generated by the magnetic field [13]. In this technique, important issues such as location of the MNPs injection points, doses, MNPs types and concentrations, and

* Corresponding author.
E-mail address: nilami@iqn.upv.es (N. Laguarda-Miró).

aspects regarding the LF-EMF sources are yet being studied and despite the theoretical advantages, there is still work to do until the therapy is accepted by the global medical community [14]. Directly linked to this end, selecting the appropriate MNPs is not obvious as there are some requirements that they must meet such as biocompatibility or the use of specific capping molecules to make them biocompatible. Thus, physical properties of the selected MNPs will condition the thermal performance and the associated mathematical model [15,16].

Despite MNPs hyperthermia is known for more than 75 years, its personalized clinical application is still being debated [17]. In the last decades, personalized therapies have advanced and significant improvements are already being published. Some of the most recent research are focused on model parameterization [18] and temperature monitoring to improve tailored-therapies [19]. Thus, some of the uncertainties limiting the hyperthermia personalized applications are being overcome [20].

In this sense, simulation environments using the finite elements method (FEM) are excellent tools to solve some of these issues [21,22], facilitating the design of personalized therapies. Virtual simulations allow treatment planning optimization as well as predicting final results [23]. Furthermore, the posed physical and biological limitations can be overcome by including the most relevant parameters in the virtual simulation conditions [24].

In this study, three different scenarios and a 3D virtual model by nonlinear Pennes bio-heat equation, perfusion and thermal tissue properties in combination with LF-EMF and MNPs have been designed to study the thermal behaviour of animal tissue samples. The aim is to provide a realistic simulation model to obtain an optimized method for a multi-site injection planning thus improving hyperthermia treatments and their clinical applications.

2. Materials and methods

The introduced model has considered three fundamental parameters: the MNPs, LF-EMF and a virtual model of cat's back with a tumour. Once the model was developed, tests were carried out in three different 3D-simulation scenarios: (a) Small dose of MNPs without diffusion, (b) Aleatory MNPs position with diffusion and (c) MNPs Distribution Plan, in the way it is explained below:

2.1. MNPs selection

Magnetite (Fe_3O_4) MNPs [25,26] were selected due to their high biocompatibility (approved by the US Food and Drug Administration) [27–29] and efficient thermal energy at relatively low field strengths (up to 400 A/m for LF-EMF) [30]. Within this type of MNPs, superparamagnetic subtype particles (SP) were selected since they are small and do not present remanence. Consequently, they permit better diffusion inside the tumour [31]. Moreover, SP-MNPs have demonstrated good behaviour in cellular environments, being an ideal factor in this therapy.

Intrinsic loss power (ILP) is the parameter characterising the heating capability of MNPs and although the MNPs performance can be extremely effective in water suspension, ILP dramatically decreases when MNPs are immersed in a cellular environment [32,33] In this sense, two loss mechanisms contribute to the overall heating: Brownian and Néel relaxations. On the one hand, Brownian relaxation time increases when viscosity in the cellular medium rises, making the Brownian loss mechanism inefficient [34]. Hence, higher frequencies are used where SP-MNPs loss is dominated by the Néel relaxation effect; however, there is certain dependence on the Brownian effect due to its morphological nature [35]. On the other hand, MNPs tend to accumulate in certain parts of the cell resulting in a dipole interaction due to their proximity.

In the conducted simulations, the maximum concentration was limited to 3% Fe w/v (155 mg/mL), assuming a linear response theory (LRT) behaviour model [36]. Finally, a thermal performance of nano-fluid (NF), extracted from different real-case reports, was provided. Thus, ILP maximum values were 4.1 nH·m²/kg in the extracellular environment and 1.75 nH·m²/kg in the intercellular environment [29,37,38].

2.2. Predictive mathematical models

Once the MNPs dose was injected, it was possible to change NF heating by changing the field properties remotely. The appropriate mathematical formulae allow heating prediction to be used both in the planning stage and in real-time while therapy is being carried out. In this scenario, many predictive mathematical models have been proposed [39,40]. Eqs. (1) and (2) developed by Rosensweig solve the problem of losses using an LRT model. Some parameters in these equations, such as anisotropy, are too complex to be theoretically obtained although their experimental determination is simpler. E.g.: Specific Absorption Rate (SAR) is a reference parameter and it is calculated *a posteriori* [41]. The purpose is to start from the experimental thermal performance conditions and then, apply variations according to the concentration and properties of the field.

$$\frac{1}{\tau_R} = \frac{1}{\tau_B} + \frac{1}{\tau_N} = \frac{k_B T}{3\eta V_h} + \frac{1}{\tau_0 e^{K_{eff} V / k_B T}} \tag{1}$$

Eq. (1) shows an expression for the effective relaxation time τ_R, where τ_B is the Brownian relaxation time, τ_N is the Néel relaxation time, k_B is the Boltzmann constant, T is the absolute temperature of the medium, η represents the fluid viscosity, V_h is the hydrodynamic volume, K_{eff} is the anisotropy constant, τ_0 is a value of time characteristic of the material (typical values are between 10^{-9} and 10^{-10} seconds) and V is the volume of MNPs.

Quantification of the power dissipation of magnetic nanoparticles in an LF-EMF is usually carried out by measuring the specific absorption rate (SAR) (also referred to a specific loss power) (see Eq. (2)),

$$SAR = \frac{\mu_0^2 M_s^2 V H_o^2}{3 k_B T \tau_R} \cdot \frac{(2\pi f \tau_R)^2}{1 + (2\pi f \tau_R)^2} \tag{2}$$

where μ_0 is the vacuum permeability, H_0 and f are the amplitude and frequency of the LF-EMF and M_s is the magnetic saturation.

The ILP is obtained by SAR normalization using the field frequency and amplitude, and is therefore independent of the magnetic field parameters ($ILP = SAR / f H_o^2$)

2.3. LF-EMF

MNPs are excited using an alternating electromagnetic field generated by field coils outside the animal's sample. Excitation frequency and amplitude are determined by a combination of MNPs size and properties, and limitations imposed by undesired exposure of normal tissue.

Field strengths and frequencies that could exceed biological limitations [42,43] are commonly used to quantify the MNPs heat losses. Various researchers have proposed simple criteria to avoid undesired eddy current heating: Among others, Hergt and Dutz [44] suggested that the product field strength (H) and frequency (f) should not exceed $C = 5x10^9$ [$Am^{-1}s^{-1}$]:

$$H \cdot f < C \tag{3}$$

However, this limit is also dependent on the field coil geometry with respect to the body, a factor that was not explicitly taken into account and hence may be excessive, as reflected in the phase I clinical trial performed by Johannsen's team [45]. In

Table 1

Simulated thermal tissue properties; where ρ, c, k, h and p are mass density, specific heat, thermal conductivity, generated heat and perfusion ratio respectively.

	$\rho[kg/m^3]$	$c[J/kg/K]$	$k[W/m/K]$	$h[W/kg]$	$p[ml/min/kg]$
Bladder	1023.61	4178.00	0.560	0.506	32.709
Blood	1049.75	3617.00	0.517	0.000	10000.000
Large Intestine	1088.00	3654.50	0.542	11.851	765.232
Cerebrospinal Fluid	1007.00	4095.50	0.573	0.000	0.000
Muscle	1090.00	3421.00	0.495	0.906	36.738
Spleen	1089.00	3596.00	0.534	24.113	1556.980
Spinal Cord	1075.00	3630.00	0.513	2.483	160.333
Fat	911.00	2348.33	0.211	0.5066	32.709
Rectum	1088.00	3763.00	0.535	11.851	765.232
Small Intestine	1030.00	3595.00	0.493	15.893	1026.250
Kidney	1066.25	3763.00	0.535	18.052	3795.030
Bone Cortical	1908.00	1312.83	0.320	0.1549	10.000
Bone Cancellous	1178.33	2274.00	0.312	0.465	30.000
Skin	1109.00	3390.50	0.372	1.64752	106.381

Table 2

Linear response perfusion data [ml/min/kg/K].

T[°C]	38	40	41	42	43.5	44	45
Muscle	52	99	-	163	0	-	-
Muscle Tumour	-1.08	-3.18	-10.87	0	-	-	-
Fat	44	83	138.1	0	-	-	-
Fat Tumour	-1.08	3.18	-10.87	0	-	-	-
Skin	141	268	637	-	-	1516	0

this case, LF-EMF application was limited to 100 kHz and 5 kA/m because of the sensations experienced by the patient. Subsequent studies determined that the maximum tolerated amplitudes depend on the application area, being in the order of 3–5 kA/m for the pelvic area, up to 8.5 kA/m for the thorax and between 3.8-13.5 kA/m for the head. Taking these results as a reference, it is stipulated that the frequency-amplitude product should not exceed 1.35×10^9 [Am^{-1}s^{-1}] [8]. In the same way, the maximum field strength was limited to tolerable limits [42,43]. Thus, a field intensity of 3.97 kA/m (5mT) was selected using a virtual solenoid inductor with 30 circular turns of 200 mm diameter and 300 mm length. The inductor reached a maximum current of 125 A at 300 kHz.

2.4. Virtual scenario

2.4.1. The cat's back model

Simulations were carried out with the virtual model of a cat presenting a tumour in the front part of the trunk with 21.51 ml and 0.405 ml of muscle and fat tissue volumes respectively. The virtual model was obtained by biomedical imaging using computerized tomography (CT) and biomedical images were segmented using the iSEG application (*ZMT, Zurich, Switzerland*). The resulting segmentation volumes were exported to the FEM environment Sim4Life (*ZMT, Zurich, Switzerland*) as it is a computational life sciences platform integrating computable phantoms with physics solvers and advanced tissue models for directly analyzing biological real-world phenomena and complex technical devices in a 3D validated biological and anatomical environment. Next, physical properties for each type of tissue were defined (Table 1) as well as perfusion values for the different tissues involved in the therapy (Table 2).

The adopted perfusion model was a linear one (as a function of the treatment temperature) thus, considering tissue thermoregulation [46,47].

Multiple 2D slices of the studied body were extracted by using biomedical imaging techniques. These sections allowed to create a 3D model of different tissues and organs by using segmentation

techniques. Once differentiated, the appropriate physical properties and perfusion behaviours were assigned to each type of tissue. Thus, the concurrent use of these elements allowed the simulation of thermal NF behaviour in the studied tissues. As a result, power density (PD) was calculated by using LRT equations and it was finally transformed into heat inside the tumour. The virtual space model was discretized using a uniform, isotropic tissue grid. In the case of the tumour, a 0.8 mm grid was set, in contrast to the rest of the tissues where a grid size of 2.5 mm was used.

Additionally, an initial and uniform temperature of 37 °C was considered for the tissues as well as a room temperature of 25 °C. The selected heat blood capacity was 4.05291 MJ/m^3/K and the animal/air thermal transmission coefficient was 6 W/m^2/K.

2.4.2. Thermal model

The thermal response of an animal's body requires a complex model [48]. Body heat is distributed from one area to another by blood flow in arteries and veins and its branching varies depending on various factors: sex, age, and even from one individual to another. The Pennes model proposes a solution using a thermal equilibrium equation which shows that the ratio of heat transferred between blood and tissues is proportional to the volumetric perfusion and the difference between the arterial blood and local tissue [49,50]:

$$C_u \frac{\partial T_u(X, t)}{\partial t} = \nabla \cdot k_u \nabla [T_u(X, t)] - \omega_b C_b T_u(X, t) + Q_m + C_b \omega_b T_a$$
$$+ Q_{np}\ (X, t) \tag{4}$$

where C_u, y C_b refer to the specific heat of tissue and blood respectively; X are the Cartesian coordinates x, y, z; t the simulation time; k_u the thermal tissue conductivity; ω_b the blood perfusion; T_u, T_a are the unfrozen tissue and arterial blood temperatures respectively; Q_m is the metabolic heat [51]; and Q_{np} the PD provided by MNPs under the action of LF-EMF [52].

2.4.3. 3D simulation scenarios

In this study, three different 3D simulation scenarios have been considered:

– Small dose of MNPs without diffusion.
– Aleatory MNPs position with diffusion.
– MNPs Distribution Plan.

The aim was to study the distribution, concentration and power loss of the MNPs under LF-EMF excitation, when the NF was injected into the tumour. After the NF injection two different scenarios were considered: (a) NF without diffusion in the tumour and (b) with NF diffusion. Finally, the best result was optimized using a new NF distribution method.
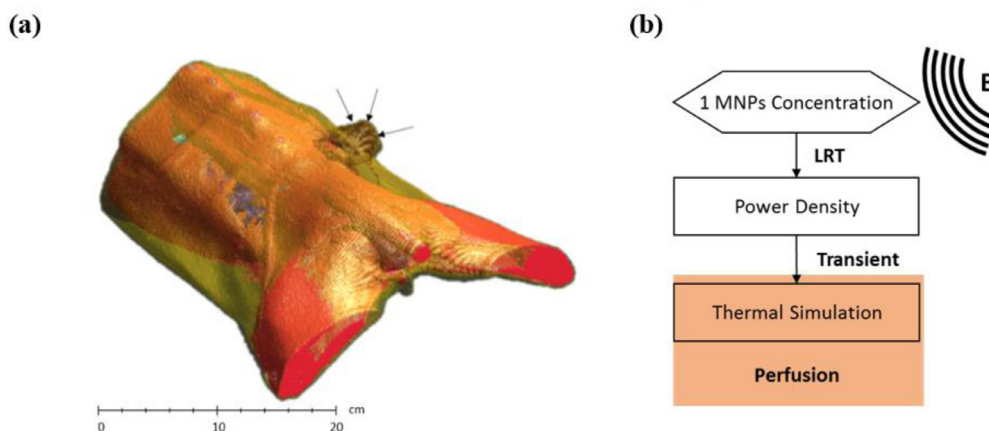
Fig. 1. (a) Virtual animal model obtained by computed tomography and detail of the injection points and (b) flowchart process.
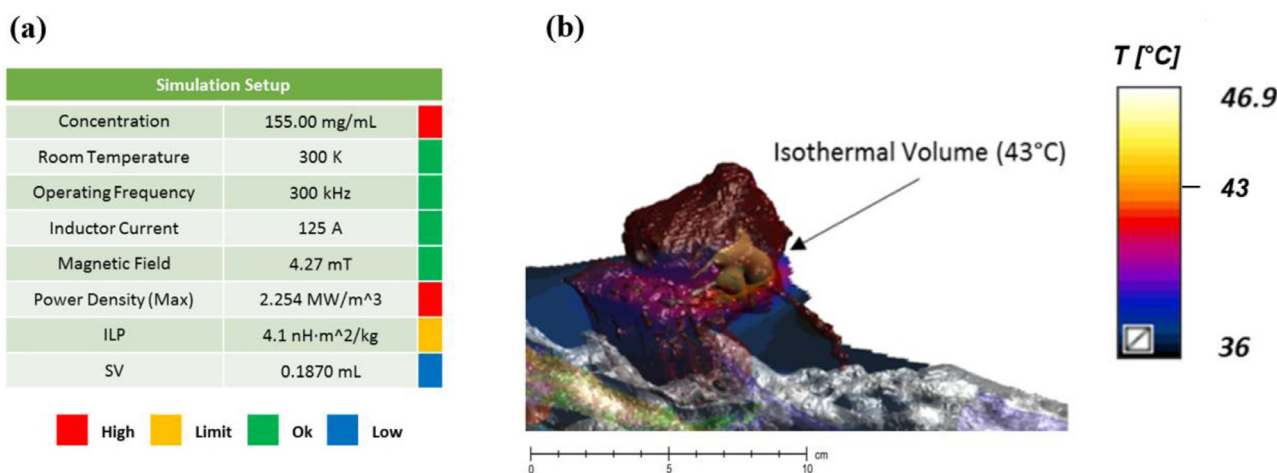

Fig. 2. (a) Simulation setup and (b) temperature distribution within the virtual tumour and isothermal volume at 43 °C.

3. Results and discussion

Simulations provided 3D temperature distributions and their evolution with time throughout the treatment (3600 s). The goal was to achieve hyperthermal temperatures in 90% of the tumour volume whilst preventing the rest of the tissues from being significantly affected. A further restriction was imposed to limit the maximum allowed temperature that was set in the range from 43 to 46 °C in order to avoid tissue ablation.

3.1. Small dose of MNPs without diffusion

In this simulation scenario, a small NF volume was injected at different tumour points (Fig. 1a). In order to take advantage of the high NF ILP in liquid base, treatment should be performed immediately after the injection. For this reason, no diffusion was considered and the proposed model only had one concentration. From this concentration and the distribution of the LF-EMF, the 3D distribution of the PD using the mathematical LRT model was calculated. The 3D PD volume was used as input data for a subsequent transient temperature simulation (Fig. 1b). The result shows the thermal evolution of the tumour over time taking into account the different physical properties and the cooling capacity of the tissues.

Fig. 2a shows the simulation setup including a colour diagram quantitatively indicating the degree of adjustment and limitations of the main parameters. The graphical result (Fig. 2b) shows how temperature was distributed within the tumour. In order achieve a better visualization, skin, fat and muscle, were hidden from the simulation. Temperature distribution within the animal tissue is represented by a colorimetric gradation along a plane. This plane cuts the median area of the tumour in which the isothermal temperature is represented by the 43 °C volume. In this case, temperature is associated with a linear scale of colours ranging from 36 to 46.9 °C.

Despite the high ILP, high MNPs and PD concentrations were required to reach an acceptable volume of hyperthermia inside the tumour [53]. Nevertheless, it must be taken into consideration that this technique could only be applied immediately after injection, since NF diffusion is immediate.

3.2. Aleatory MNPs position with diffusion

Opposite to the previous case, NF diffusion after injection was expected in this scenario. To counteract the low ILP due to the dispersion in the cellular environment, the injected suspension volume (SV) was increased to that used in clinical trials (from 0.28 ml/cm^3 to 0.4 ml/cm^3 of tumour) [54,55]. Once NF is applied to the tumour, diffusion through the intercellular space starts in a theoretical Gaussian form [56].

As shown in Fig. 3a, the simulation configuration was set maintaining both inductor current and electromagnetic field intensity
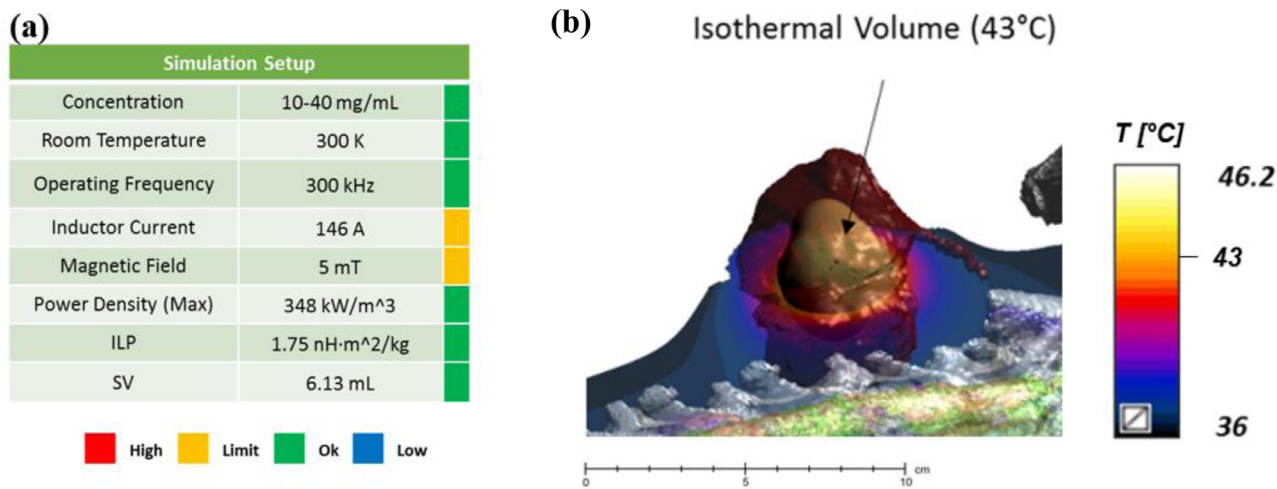
Fig. 3. (a) Simulation setup and adjustment to the limit values and (b) temperature distribution within the virtual tumour and isothermal volume at 43 °C.
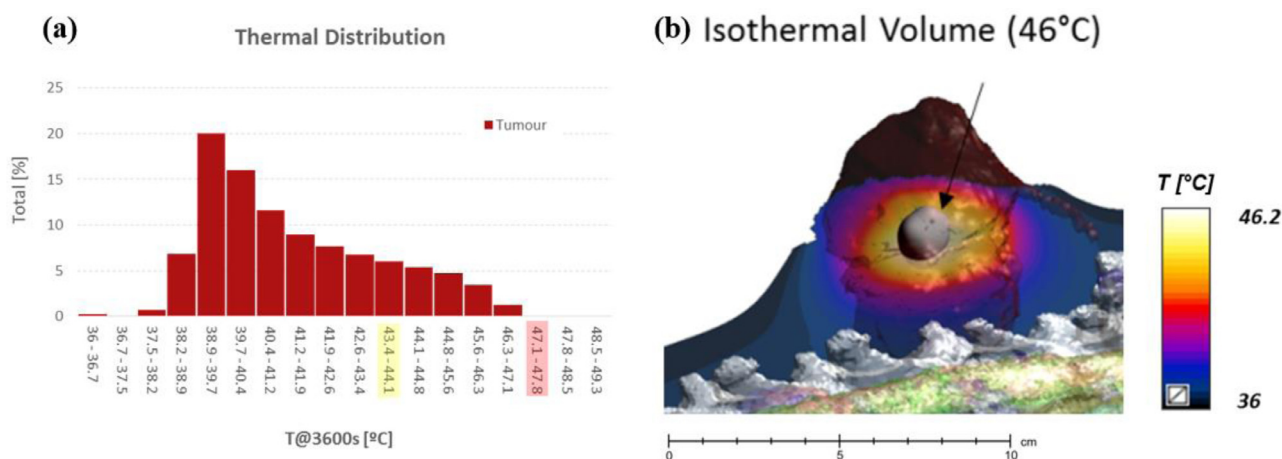

Fig. 4. (a) Temperature distribution histogram and (b) graphical thermal distribution of the isothermal volume at 46 °C.
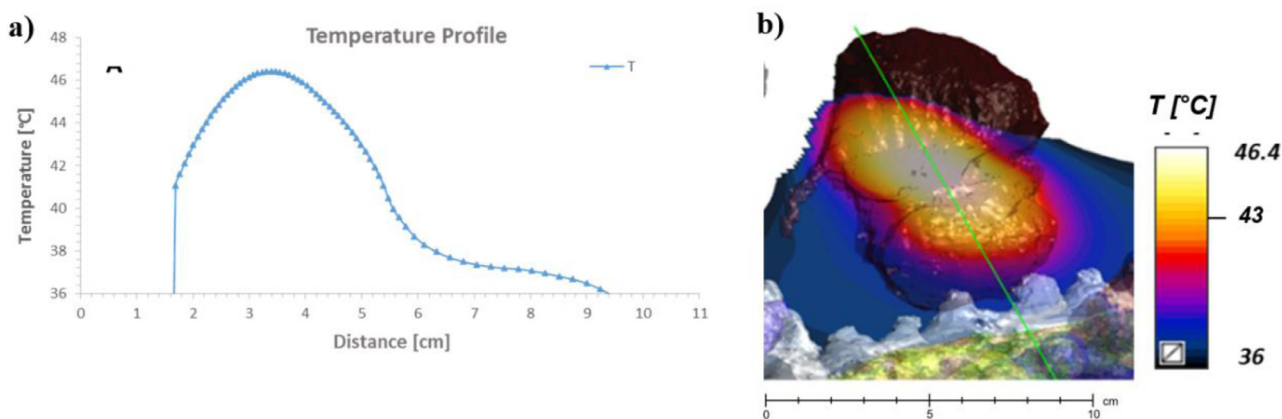

Fig. 5. (a) Graphical temperature distribution when the average tumour temperature reaches 43 °C and (b) transverse thermal profile recorded by the green line.

at their limits. As observed in Fig. 3b, the hyperthermia volume reached was higher than the one obtained in the previous scenario (Fig. 2a). Nevertheless, the hyperthermia volume did not exceed 25% of the tumour still being far away from the target (90% of the tumour volume).

A strategy to raise the obtained hyperthermia volumes is to increase PD. For this purpose, either the LF-EMF intensity or the initial injection concentrations must be increased. In this sense, the proposed configuration does not allow the field intensity to increase, since it is at the limit, but it would allow an increase in concentration. This effect can be appreciated in the volumetric histogram of temperature distribution within the tumour. Consequently, if PD raises, temperature in the hyperthermia volume >43 °C also increases (yellow mark), as well as heat in the hotspot thus, having a hotspot volume in the ablation area (red mark) (Fig. 4).
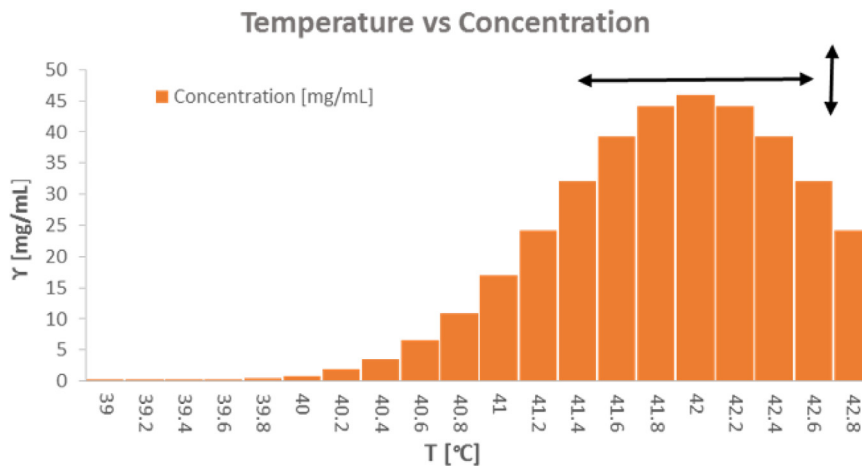
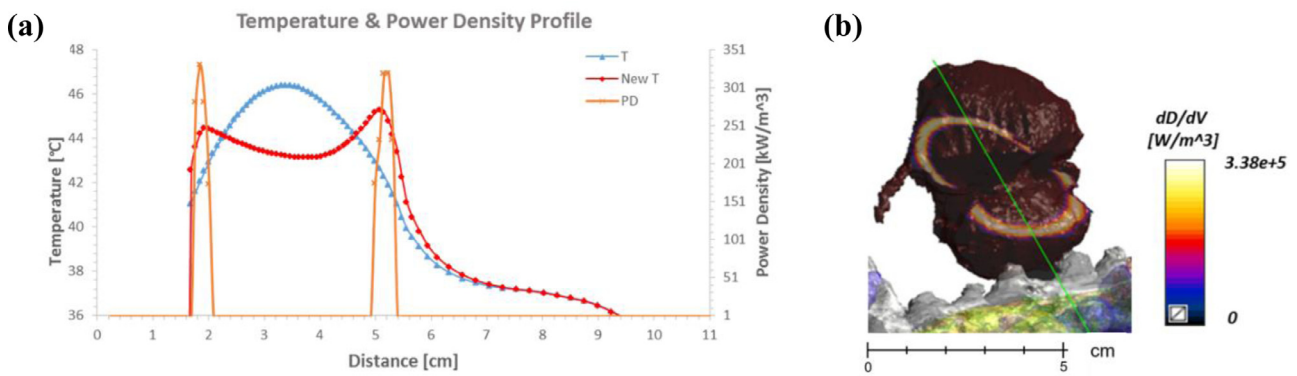**Fig. 6.** Distribution of the MNPs concentration vs temperature.

Fig. 7. (a) Cross section of the thermal profile along the green line recorded in the first step (blue) and in the second step (red) and the new DP distribution (orange). (b) 3D PD distribution.
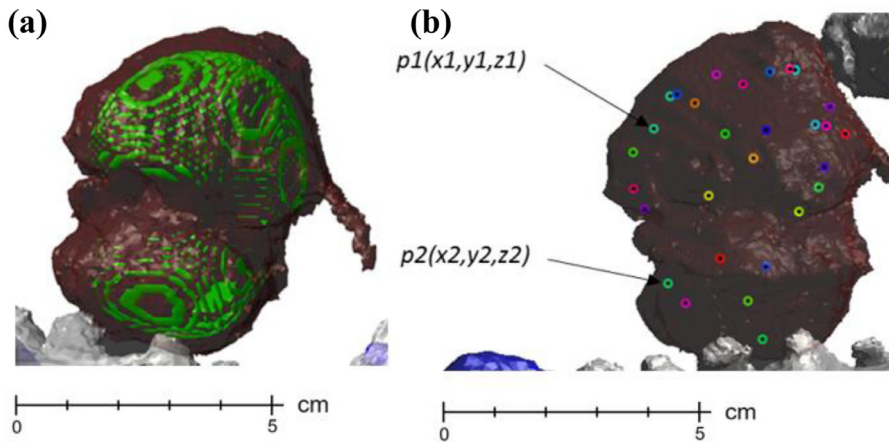

Fig. 8. (a) Highest NF concentration volume and (b) positioning of 28 injection points.

3.3. MNPs distribution plan

The strategy in the previous scenario meant a considerable improvement in the obtained hyperthermia volume. However, it was appreciated that performing a random NF distribution was not a good option in a scenario affected by many factors such as tumour morphology, different thermal properties of tissues and perfusions, thermal NF performance, field properties, etc. In order to improve these results, a method capable of solving this problem and able to be an application pattern is required.

Salloum et al. proposed an iterative algorithm in which an index is optimized in order to reach hyperthermia temperature within the tumour, depending on the number of predetermined injection points and assuming a NF Gaussian distribution [56,57]. Undoubtedly, the obtained results meet the expectations. However, working in a 3D scenario with a large number of injection points would be computationally very demanding [58,59].

The proposed planning method (Fig. 10) was based on a different concept as it aimed to find an optimal NF distribution able to reduce the number of injection points as well as considering
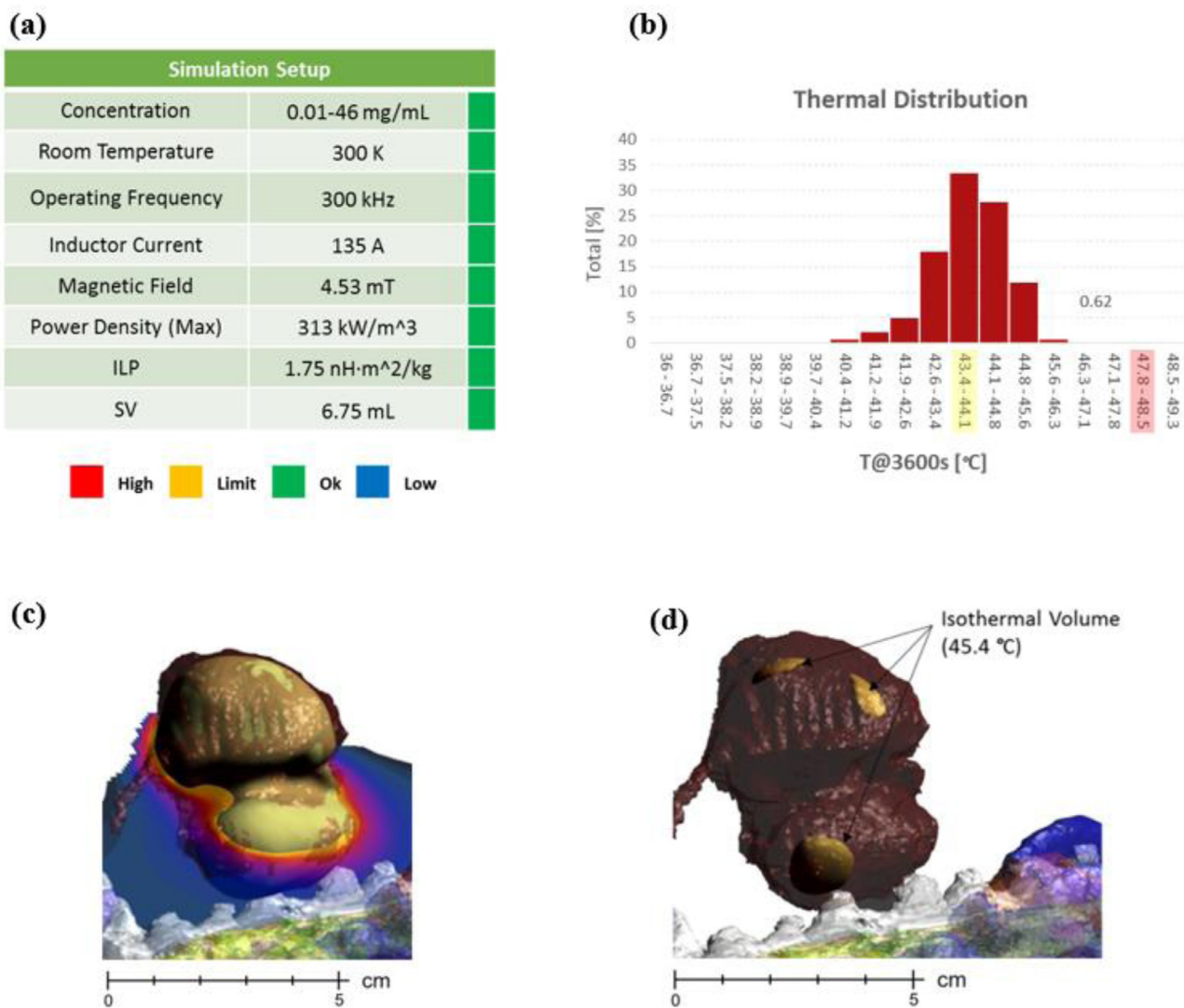
Fig. 9. (a) Configuration table. (b) Volumetric histogram of the temperature distribution inside the tumour (upper right). (c) Graphical thermal distribution result in the virtual model and isothermal volume at 43 °C. (d) Isothermal volume at 45.4 °C.

their position, concentration, volume and the LF-EMF parameters and also taking into account the physical properties of the tissues and their different perfusions. A specific goal for this method was to reduce the computation requirements in order to perform simulations in a reasonable computation time [60].

3.3.1. Optimization method

1. A uniformly distributed PD throughout the tumour volume and a transient thermal response was simulated. The simulation was iterated by varying the PD until the mean tumour volume temperature reached 43°C. With this result, we obtained a characteristic three-dimensional map.

2. The temperature map obtained was taken as a reference to generate a new distribution of the MNPs and produce a new PD map. The result was included in the simulation model and a transient thermal simulation was performed. The algorithm was iterated by varying the Gaussian distribution profile of concentrations until it was adjusted better to a volume of hyperthermia (43 °C) that approached the target set. It was necessary to verify that the rest of the tissues remained minimally affected by the thermal dose.

3. Once the model was adjusted, it was possible to extract the position of the injection points taking the maximum MNPs volume concentration as a reference.

4. Finally, SV and concentration in the injection points were deduced from the 3D NF distribution.

In the first step of this method, a characteristic pattern of temperature distribution was obtained when the tumour reached 43 °C. In fact, Fig. 5b is a thermographic section showing remarkably higher temperatures inside the tumour than in the peripheral area as well as temperature decrease much more pronounced in the tissues positioned close to the skin and muscle due to their greater perfusion capacity (Fig. 5a).

The second step consisted in performing a new NF distribution concentration depending on the temperature. The procedure consisted of increasing the concentration in the points where the temperature was lower and *vice versa*. For the NF diffusion simulation, 20 different distribution concentrations were taken following a Gaussian pattern using Eq. (5). Another consideration was to prevent the NF from being deposited too close to the superficial cortex of the tumour, trying to minimise the effect on the tissues adjacent to the tumour. Handling these parameters, the intention
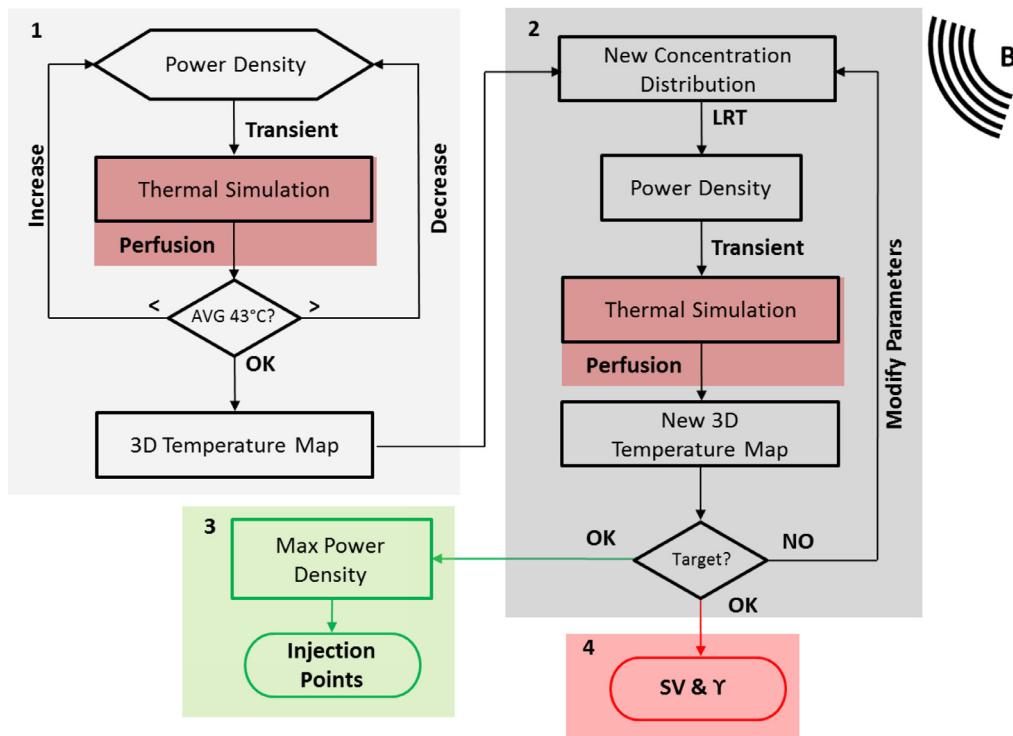
Fig. 10. Flowchart process of the new MNPs distribution method showing the different steps and stages.

was to maximize the volume of hyperthermia within the tumour and to minimize the heat dose in the rest of the tissues.

Automation of this process consisted in displacing the Gaussian crest to the left or the right. This permits control of the depth of the NF injection and thereby affects the adjacent tissues and the appearance of hot spots to a lesser extent. On the other hand, increasing or decreasing the concentration and/or intensity of the LF-EMF directly influenced the PD in order to adapt the volume to the tumour (Fig. 6).

$$C_i = C_{Max} \cdot e^{\left(\frac{-(i - n_{con})^2}{n_{con}^2}\right)} \tag{5}$$

where C_i is the concentration, C_{Max} is the maximum concentration, n_{con} is the number of concentrations; i is a number from 0 to (n_{con}-1).

The NF pattern distribution was transformed into a PD through the LRT model, obtaining the 3D distribution as shown in Fig. 7b. The 2D graph representing the temperature was added to the PD distribution and the new thermal response after a transient simulation. As shown, the thermal stimulus was compensated around the hyperthermia temperature (Fig. 7a).

The third step was to deduce the ideal injection points. These points are connected to the maximum MNPs concentration, and they indicate their exact positions (Fig. 8).

The last step consisted in determining volume and concentration of the initial injection from the highest concentration distribution. For the selection, a total volume and concentration of the suspension, lower than the maximum limit (155 mg/ml and 0.4 ml/cm³ of tumour) should be considered. In addition, it should be taken into account that the initial concentration was higher than the maximum obtained, since it was expected to be diffused later.

As shown in Fig. 9, all the experimental parameters are within the optimal limits. The histogram shows a volumetric distribution around the hyperthermia temperature (yellow mark) avoiding ablation of the tissues (red mark). As for the graphical results, hyperthermia volume is perfectly adapted to the tumour morphology and the area affected by the heat located in the peripheral tissues was minimal. As for hot spots, they also appear but only when 90% of the hyperthermia volume has already been reached within the tumour, so this a limiting factor cannot be considered.

4. Conclusions

The present work focuses on the development of a tailor-made planning for MNPs mediated hyperthermia therapy in various simulation situations. Different elements were included, modelling the main characteristics and limitations. The simulation model was based on three different scenarios. The results showed that NF worked in an isolated way when there was no diffusion, generating localized heat close to the volume it occupied. As a consequence, a high PD was needed to obtain a minimum hyperthermia volume. Therefore, for this heating to be properly distributed throughout the tumour volume, an internal NF diffusion was necessary. Diffusion in the cellular environment implies a reduction of the calorific power, which was counteracted with a higher NF volume. The result was a much higher hyperthermia volume requiring both lower field strengths and concentrations than in the previous scenario. However, one of the limitations in reaching a higher hyperthermia volume was the presence of hot spots within the tumour caused by poor NF distribution. Finally, the last optimized distribution method serves as a pattern in order to reach 90% hyperthermia volume, minimally affecting to the rest of the tissues.

In the simulations, NF was supposed to reach its maximum concentration around the injection point with a constant diffusion taking a Gaussian pattern. However, the MNPs were dispersed differently to the theoretical homogeneous tissue case, and it was due to the irregularities within the tumour. For this reason, predicting MNPs exact distribution was complex. Therefore, it would have been interesting to obtain the actual distribution map through biomedical imaging techniques, once the NF was injected following the described pattern.

Once the MNPs concentration is determined, it can be used to recalculate the temperature distribution and can later serve as a reference to guide future injection positions. Nevertheless, the number of points will be set depending on the accessibility and diffusion inside the tumour. As a complete virtual model of the affected tissue and surroundings is at our disposal, a study to guess how different positions could be reached and to assess the most appropriate position could be conducted. Additionally, diffusion experimental data inside the tumour would also be vital for point position determination.

The described optimal MNPs distribution method does not imply high computational cost, the result can be obtained in minutes. However, these results depend on the spatial resolution and the used processing machine. Although the present study has not focused on deducing the computational cost of the processing, we can state that the waiting time of the planning would not imply a significant delay in treatment.

Declaration of Competing Interest

The authors declare no conflict of interest.

Acknowledgments

References

[1] A. Andreozzi, L. Brunese, M. Iasiello, et al., Numérica análisis of the pulsating heat source effects in a tumor tissue, Comput. Methods Prog. Biomed. 200 (2020) 105887, doi:10.1016/j.cmpb.2020.105887.

[2] A. Rajan, N.K. Sahu, Review on magnetic nanoparticle-mediated hyperthermia for cancer therapy, J. Nanopart. Res. 22 (2020) 319, doi:10.1007/s11051-020-05045-9.

[3] A. Chicheł, J. Skowronek, M. Kubaszewska, et al., Hyperthermia – description of a method and a review of clinical applications reports, Pract. Oncol. Radiother. 12 (2007) 267–275.

[4] A.S Garanina, V.A Naumenki, A.A Nikitin, et al., Temperature-controlled magnetic nanoparticles hyperthermia inhibits primary tumor growth and metastases dissemination, Nanomed. Nanobiotechnol. 25 (2020) 102171.

[5] E. Oberacker, C. Diesch, J. Nadobny, et al., Specific planning for thermal magnetic resonance of glioblastoma multiforme, Cancers 13 (2021) 1867, doi:10.3390/cancers13081867.

[6] J. Van der Zee, Heating the patient: a promising approach? Ann. Oncol. 13 (2002) 1173–1184.

[7] A. Singh, S. Jain, S.K. Sahoo, et al., Magnetic nanoparticles for amalgamation of magnetic hyperthermia and chemotherapy: an approach towards enhanced attenuation of tumor, Mater. Sci. Eng. C 110 (2020) 110695.

[8] S. Hatamie, Z.M Balasi, M.M. Ahadian, et al., Hyperthermia of breast cancer tumor using graphene oxide-cobalt ferrite magnetic nanoparticles in mice, J. Drug Deliv. Sci. Technol. 65 (2021) 102680.

[9] M.H. Capstick, M. Gosselin, E. Neufeld, et al., Novel applicator for local RF hyperthermia treatment using improved excitation control, in: Proceedings of the 31th URSI General Assembly and Scientific Symposium (URSI GASS), 2014, pp. 1–4.

[10] M.R. Bailey, V. Khokhlova, O. Sapozhnikov, et al., Physical mechanisms of the therapeutic effect of ultrasound (a review), Acoust. Phys. 49 (2003) 369–388.

[11] A. Dahaghin, S. Emadiyanrazavi, M. Salimibani, et al., A numerical investigation into the magnetic nanoparticles hyperthermia cancer treatment injection strategies, Biocybern. Biomed. Eng. 41 (2021) 516–526.

[12] B.E. Kashevsky, S.B. Kashevsky, V.S. Korenkov, et al., Magnetic hyperthermia with hard-magnetic nanoparticles, J. Magn. Magn. Mater. (2014) 1–6.

[13] N.T.K. Thanh, A. Hervault, Magnetic nanoparticle-based therapeutic agents for thermo-chemotherapy treatment of cancer, Nanoscale (2014) 11553–11573.

[14] G.P. Szigeti, O. Szasz, G. Hegyi, Personalised dosing of hyperthermia, J. Cancer Diagn. 1 (2016) 107.

[15] N. Mahesh, N. Singh, P. Talukdar, A mathematical model for understanding nanoparticle biodistribution after intratumoral injection in cancer tumors, J. Drug Deliv. Sci. Technol. 68 (2022) 103048.

[16] P. Shojaee, H. NIroomand- Oscuii, M. Sefidgar, et al., Effect of nanoparticle size, magnetic intensity, and tumor distance on the distribution of the magnetic nanoparticles in a heterogeneous tumor microenvironment, J. Magn. Magn. Mater. 498 (2022) 166089.

[17] M. Peraivi, H. Eslami, et al., Magnetic hyperthermia: potentials and limitations, J. Indian Chem. Soc. 99 (2022) 100269, doi:10.1016/j.jics.2021.100269.

[18] J. Nadobny, A. Lim, et al., Improved patient-specific hyperthermia planning based on parameterized electromagnetic and thermal models for the SIGMA-30 applicator, Ing. J. Hyperther. 38 (1) (2021) 663–678, doi:10.1080/02656736.2021.1909757.

[19] J. Kosir, D. Vella, Towerds personalized and versatile monitoring of temperatura fields within heterogeneous tissues during laser therapies, Biomed. Opt. Express 12 (7) (2021) 4530–4543, doi:10.1364/BOE.428028.

[20] S. Gavazzi, A.L.H.M.V. Van Lier, et al., Advanced patient spedific hyperthermia treatment planning, Ing. J. Hyperth. 37 (1) (2020) 992–1007, doi:10.1080/02656736.2020.1806361.

[21] M. Sefidgar, E. Bashooki, P. Shojaee, Numerical simulation of the effect of necrosis area in systemic delivery of magnetic nanoparticles in hyperthermia cancer treatment, J. Therm. Biol. 94 (2020) 102742.

[22] S.R. Gunkala, V.M. Job, S. Sakhamuri, et al., Numerical study of blood perfusion and nanoparticle transport in prostate and muscle tumours during intravenous magnetic hyperthermia, Alex. Eng. J. 60 (2021) 859–876.

[23] M. Suleman, S. Riaz, 3D in silico study of magnetic fluid hyperthermia of breast tumor using Fe₃O₄ magnetic nanoparticles, J. Therm. Biol. 91 (2020) 102635.

[24] B. Gheflati, N. Naghavi, Computational study of nanoparticle assisted hyperthermia in tumors embedded with large blood vessels, Int. J. Heat Mass Transf. 151 (2020) 119415.

[25] C.S. Brazel, Magnetothermally-responsive nanomaterials: Combining magnetic nanostructures and thermally-sensitive polymers for triggered drug release, Pharm. Res. 26 (2009) 644–656.

[26] R.S. Ningthoujam, R.K. Vatsa, A. Kumar, et al., Functionalized magnetic nanoparticles: concepts, synthesis and application in cancer hyperthermia, Funct. Mater. (2012) 229–260.

[27] A.K. Hauser, R.J. Wydra, N.A. Stocke, et al., Magnetic nanoparticles and nanocomposites for remote controlled therapies, J. Control. Release 219 (2015) 76–94.

[28] I. Hilger, R. Hergt, W.A. Kaiser, Towards breast cancer treatment by magnetic heating, J. Magn. Magn. Mater. 293 (2005) 314–319.

[29] I. Marcos-Campos, L. Asín, T.E Torres, et al., Cell death induced by the application of alternating magnetic fields to nanoparticle-loaded dendritic cells, Nanotechnology 22 (2011) 205101.

[30] S. Ruta, R. Chantrell, O. Hovorka, Unified model of hyperthermia via hysteresis heating in systems of interacting magnetic nanoparticles, Sci. Rep. 5 (2015) 9090.

[31] C.L. Dennis, R. Ivkov, Physics of heat generation using magnetic nanoparticles for hyperthermia, Int. J. Hyperth. 29 (2013) 715–729.

[32] M. Kallumadil, M. Tada, T. Nakagawa, et al., Suitability of commercial colloids for magnetic hyperthermia, J. Magn. Magn. Mater. 321 (2009) 1509–1513.

[33] Ota, S., Trisnanto, S.B., Takeuchi, S., et al. (2021). Quantitation method of loss powers using commercial magnetic nanoparticles based on superparamagnetic behavior influenced by anisotropy for hyperthermia. 538: 168313.

[34] S. 23Dutz, R. Hergt, Magnetic nanoparticle heating and heat transfer on a microscale: Basic principles, realities and physical limitations of hyperthermia for tumour therapy, Int. J. Hyperth. 29 (2013) 790–800.

[35] M. Ma, Y. Wu, J. Zhou, et al., Size dependence of specific power absorption of Fe₃O₄ particles in AC magnetic field, J. Magn. Magn. Mater. 268 (2004) 33–39.

[36] Z. Nemati, J. Alonso, L.M. Martinez, et al., Enhanced magnetic hyperthermia in iron oxide nano-octopods: size and anisotropy effects, J. Phys. Chem. C 120 (2016) 8370–8379.

[37] Q. Pankhurst, N.T.K. Thanh, S.K. Jones, et al., Progress in applications of magnetic nanoparticles in biomedicine, J. Phys. D Appl. Phys. 42 (2009) 224001.

[38] M. Suto, Y. Hirota, H. Mamiya, et al., Heat dissipation mechanism of magnetite nanoparticles in magnetic fluid hyperthermia, J. Magn. Magn. Mater. 321 (2009) 1493–1496.

[39] J.P. Fortin, C. Wilhelm, J. Servais, et al., Size-sorted anionic iron oxide nanomagnets as colloidal mediators for magnetic hyperthermia, J. Am. Chem. Soc. 129 (2007) 2628–2635.

[40] R.E.E. Rosensweig, Heating magnetic fluid with alternating magnetic field, J. Magn. Magn. Mater. 252 (2002) 370–374.

[41] R. Di Corato, A. Espinosa, L. Lartigue, et al., Magnetic hyperthermia efficiency in the cellular environment for different nanoparticle designs, Biomaterials 35 (2014) 6400–6411.

[42] V.M. Khot, B. Salunkhe, N.D. Thorat, et al., Induction heating studies of combustion synthesized MgFe₂O₄ nanoparticles for hyperthermia applications, J. Magn. Magn. Mater. 332 (2013) 48–51.

[43] C. Martinez-Boubeta, K. Simeonidis, A. Makridis, et al., Learning from nature to improve the heat generation of iron-oxide nanoparticles for magnetic hyperthermia applications, Sci. Rep. 3 (2013) 1652.

[44] R. Hergt, S. Dutz, Magnetic particle hyperthermia-biophysical limitations of a visionary tumour therapy, J. Magn. Magn. Mater. 311 (2007) 187–192.

[45] M. Johannsen, U. Gneveckow, L. Eckelt, et al., Clinical hyperthermia of prostate cancer using magnetic nanoparticles: presentation of a new interstitial technique, Int. J. Hyperth. 21 (2005) 637–647.

[46] I. Laakso, A. Hirata, Dominant factors affecting temperature rise in simulations of human thermoregulation during RF exposure, Phys. Med. Biol. 56 (2011) 7449–7471.

[47] M. Murbach, E. Neufeld, M. Capstick, et al., Thermal tissue damage model analyzed for different whole-body SAR and scan durations for standard MR body coils, Magn. Reson. Med. 71 (2014) 421–431.

[48] C. Zhang, D.T. Johnson, C.S. Brazel, Numerical study on the multi-region bio-heat equation to model magnetic fluid hyperthermia (MFH) using low curie temperature nanoparticles, IEEE Trans. Nanobiosci. 7 (2008) 267–275.

[49] H.H. Pennes, Analysis of tissue and arterial blood temperatures in the resting human forearm, Appl. Physiol. 85 (1948) 93–122.

[50] E.H. Wissler, Pennes' 1948 paper revisited, J. Appl. Physiol. 85 (1998) 35–41.

[51] Engineering IJI. (2011). Parallel algorithms for freezing problems during cryosurgery 11–9.

[52] Z.Z. He, X. Xue, J. Liu, An effective finite difference method for simulation of bioheat transfer in irregular tissues, J. Heat Transf. 135 (7) (2013).

[53] A. Cervadoro, C. Giverso, R. Pande, et al., Design maps for the hyperthermic treatment of tumors with superparamagnetic nanoparticles, PLoS One 8 (2013) 1–14.

[54] B. Thiesen, A. Jordan, Clinical applications of magnetic nanoparticles for hyperthermia, Int. J. Hyperth. 24 (2008) 467–474.

[55] K. Maier-Hauff, F. Ulrich, D. Nestler, et al., Efficacy and safety of intratumoral thermotherapy using magnetic iron-oxide nanoparticles combined with external beam radiotherapy on patients with recurrent glioblastoma multiforme, J. Neurooncol. 103 (2011) 317–324.

[56] M. Salloum, R.H. Ma, D. Weeks, L. Zhu, Controlling nanoparticle delivery in magnetic nanoparticle hyperthermia for cancer treatment: experimental study in agarose gel, Int. J. Hyperth. 24 (2008) 337–345.

[57] A. Attaluri, R. Ma, Y. Qiu, et al., Nanoparticle distribution and temperature elevations in prostatic tumours in mice during magnetic nanoparticle hyperthermia, Int. J. Hyperth. 27 (2011) 491–502.

[58] M. Salloum, R. Ma, L. Zhu, Enhancement in treatment planning for magnetic nanoparticle hyperthermia: optimization of the heat absorption pattern, Int. J. Hyperth. 25 (2009) 309–321.

[59] A. Attaluri, R. Ma, L. Zhu, Using MicroCT imaging technique to quantify heat generation distribution induced by magnetic nanoparticles for cancer treatments, J. Heat Transf. 133 (2011) 11003 1.

[60] R. Torchio, A. Arduino, L. Zilberti, et al., A fast tool for the parametric analysis of human body exposed to LF electromagnetic fields in biomedical applications, Comput. Methods Prog. Biomed. 214 (2022) 106543, doi:10.1016/j.cmpb.2021.106543.